Geomechanics for Energy and the Environment 39 (2024) 100575

Contents lists available at ScienceDirect

Geomechanics for Energy and the Environment

journal homepage: www.elsevier.com/locate/gete

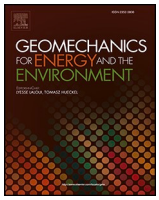

A methodology for incorporating thermal interference in the design of thermo-active pile groups

Ryan Yin Wai Liu [*,1], David M.G. Taborda [2]

Department of Civil and Environmental Engineering, Imperial College London, London, United Kingdom

ARTICLE INFO

Keywords:
Design methods
Shallow geothermal
Thermo-active piles
Thermal performance

ABSTRACT

This paper introduces innovative practical methodologies for evaluating the thermal performance of thermo-active pile groups. First, a streamlined approach for determining G-functions within such groups, based on the G-function of a single thermo-active pile is introduced. This is accomplished through a newly introduced thermal interaction factor for G-functions quantifying the increase in temperature when a pile is subjected to thermal interference from another pile. Subsequently, the paper proposes a method for calculating the power of piles within thermo-active pile groups when subjected to transient inlet temperatures. A thermal interaction factor for power is derived, quantifying the power reduction resulting from thermal interference due to another pile operating in the vicinity. These simplified methodologies are shown to reproduce the thermal performance of pile groups simulated using three-dimensional thermo-hydraulic analyses with excellent levels of accuracy without the associated computational cost. Finally, the proposed design process is applied to a 3 × 3 thermo-active pile group subjected to transient thermal loads, yielding accurate estimations of power, G-functions, and temperature changes of the thermo-active pile group. Overall, these simplified methodologies offer a robust framework for evaluating and optimising the thermal performance of thermo-active pile systems.

1. Introduction

Thermo-active piles represent a distinct advancement over conventional piles, as they not only offer structural stability but also function as ground source heat exchangers, providing buildings with low carbon heating and cooling capabilities. The adoption of thermo-active piles has witnessed a surge in popularity in recent years,[24,3,33] driven by increasingly stringent sustainability targets, such as the Merton Rule, which mandates on-site renewable energy generation for buildings,[26,37] and the overarching commitment to achieve net-zero greenhouse gas emissions by 2050. This technology is of particular significance in densely urbanised regions, where, due to the congested built environment, thermo-active piles emerge as the most viable renewable energy option.

The operation of thermo-active piles and other structures, such as retaining walls and tunnel linings, leads to differential expansion between the concrete and the surrounding ground. This results in additional shear stresses at the soil-structure interface and, therefore, internal forces are generated within the pile, as well as leading to additional ground movements that need to be considered in their design. These interaction mechanisms have been observed and, crucially, quantified in field investigations (e.g. Brandl[4]; Laloui et al.[17]; Bourne-Webb et al.[5]) and centrifuge tests (e.g. Stewart & McCartney[34]; Ng et al.[28]; Ng et al.[29]). Several numerical studies have been conducted to establish the importance of these additional forces in the design of thermo-active pile foundations, focusing not only on their magnitude but also on the modelling approach adopted for the soil and the effect of transient thermal loading (e.g. Di Donna & Laloui[8]; Gawecka et al.[11]; Iodice et al.[13]). The findings from research on the geotechnical behaviour of this type of foundations is systematically organised in a simple framework proposed in Amatya et al.[2] and Bourne-Webb et al.[6]. Clearly, at the centre of assessing the response of thermo-active piles, both in terms of thermal performance and thermo-mechanical response, is the need to establish the temperature field resulting from their operation (e.g. Sailer et al.[32], Liu et al.[18]).

In terms of thermal performance of thermo-active piles, its accurate quantification is vital to ensure they meet the heating and cooling demands of buildings. Previous studies, both numerical (e.g. Gao et al.[10]; Loveridge & Powrie[22]; Liu et al.[18]) and field-based (e.g. Park et al.[30];

* Correspondence to: Imperial College London, Room 430, Skempton Building, London SW7 2AZ, United Kingdom.
E-mail address: ryl13@ic.ac.uk (R.Y.W. Liu).
[1] ORCID: 0000-0002-5278-6426.
[2] ORCID: 0000-0001-5391-2087.

https://doi.org/10.1016/j.gete.2024.100575
Received 27 October 2023; Received in revised form 9 June 2024; Accepted 25 June 2024
Available online 28 June 2024

Nomenclature

A	A coefficient for TIF_G or TIF_P
B_1	A coefficient for TIF_G or TIF_P
B_2	A coefficient for TIF_G or TIF_P
C_1	A coefficient for TIF_G or TIF_P
C_2	A coefficient for TIF_G or TIF_P
ETE	Pile edge-to-pile edge distance
k	Thermal conductivity
k_{soil}	Thermal conductivity of the soil
L	Pile length
N_{piles}	Total number of piles in a pile group
n	Time step number being evaluated
$n_{U-loops}$	Number of U-loops within the thermo-active pile
$\overline{P}$	Normalised power per unit pile length or applied heat flux per unit pile length
$\overline{P}_{i,group}$	Normalised power of pile i within a thermo-active pile group
$\overline{P}_{single}$	Normalised power of a single thermo-active pile
Q	Flow rate of the carrier fluid
r	Radial distance
r_b	Radius of pile
r_{pipes}	The radial distance measured from the pile centre at which the pipes are located within the thermo-active pile
SF	Spacing factor
T_{in}	Inlet fluid temperature
T_{out}	Outlet fluid temperature
TIF_G	Thermal interaction factor for G-functions
TIF_P	Thermal interaction factor for power
t	Time
ΔT_{wall}	Average change in temperature at pile wall
ρC_p	Volumetric heat capacity
$\rho_f C_{p,f}$	Volumetric heat capacity of the carrier fluid
Φ_g	G-function
$\Phi_{i,group}$	G-function of pile i within a thermo-active pile group
Φ_{single}	G-function for a single thermo-active pile

Zhao et al.[40]; Jensen-Page et al.[14]), have investigated the thermal performance of individual thermo-active piles. However, it is essential to recognise that thermo-active piles are often employed in groups. It has been shown numerically,[1,12,16,19,23,25,36] in centrifuge tests[27] and in field tests[15,39] that when thermo-active piles operate together, these piles experience thermal interference effects, leading to a deterioration in their overall thermal performance compared to operating in isolation. Thermal interference arises as heat exchange between a thermo-active pile and the surrounding soil relies on the thermal gradient between them. When neighbouring piles heat up or cool down the surrounding soil, its capacity to exchange heat diminishes, resulting in reduced performance for the group as a whole.

To estimate accurately the thermal performance of thermo-active piles, it is vital to account adequately for the effects of thermal interference. Currently, the thermal performance of thermo-active piles is typically quantified in one of the two following ways:

1. The first approach involves prescribing the carrier fluid with an inlet temperature while measuring the outlet temperature to quantify the heat extracted from or injected into the ground by the thermo-active pile. This is represented as a normalised power per pile length, denoted as $\overline{P}\,[W \bullet m^{-1}]$, using Eq. (1), where $\rho_f C_{p,f}$ $\left[J \bullet m^{-3} \bullet K^{-1}\right]$ is the volumetric heat capacity of the carrier fluid, $Q\left[m^3 \bullet s^{-1}\right]$ is the flow rate of the fluid, $L[m]$ is the pile length, $(T_{in} - T_{out})$ $[K]$ is the temperature differential between the pipe inlet(s) and outlet(s), and $n_{U-loops}$ is the number of U-loops within the pile. Obviously, a thermo-active pile with better thermal performance is characterised by a higher normalised power per pile length. Studies have demonstrated that when thermo-active piles operate as a group, the temperature differential $(T_{in} - T_{out})$, and hence the power for each pile decrease due to overlapping temperature fields caused by thermal interference.[16,21,25,36,39]

$$\overline{P} = \sum_{i}^{n_{U-loops}} \frac{\rho_f C_{p,f} \bullet Q_i}{L} \bullet (T_{in} - T_{out})_i \tag{1}$$

2. The second approach involves injecting a constant heat flux into the thermo-active pile and measuring the resulting temperature increase over time. The results are then presented in a normalised format as G-functions. A thermo-active pile with inferior thermal performance exhibits a more substantial temperature change for a given heat flux, as this corresponds to a greater temperature change in the carrier fluid, ultimately reducing the efficiency of the heat pump. Moreover, an increased temperature change within the soil signifies a diminished capacity to exchange heat with the pile. Studies have indicated that multiple piles operating in proximity generate higher temperatures compared to a single pile,[1,15,19,23,39] thus necessitating the quantification of thermal interference effects.

For the first approach, Liu & Taborda[21] have developed a simplified method that enables the determination of the power of piles within a thermo-active pile group based on the power of a single pile. However, its applicability is constrained to scenarios involving thermal loads characterised by constant inlet temperatures. For the second approach, a theoretical study conducted by Loveridge & Powrie[23] has demonstrated that average G-functions for thermo-active pile groups can be determined through superposition of G-function values obtained from single piles at different radial distances from the pile.

This paper is driven by two primary objectives. Firstly, in Section 2, a simplified methodology for determining G-functions for thermo-active pile groups is introduced. The key input for this streamlined approach is the G-function pertaining to an individual pile with the same geometry as those in the pile group, evaluated solely at the pile edge. Through the application of the proposed empirically derived equation and the principle of superposition, the G-function of each pile within pile groups of any pile arrangement can be determined. The simplified methodology is subsequently validated using 3D transient thermal analyses. Secondly, in Section 3, the determination of power for piles within thermo-active pile groups is extended to accommodate thermal loads characterised by transient inlet temperatures, such as those observed as a result of realistic heat pump operational patterns. This extended method is then validated through its application to a 3×3 thermo-active pile group subjected to a time-varying thermal load. Finally, in Section 4, a practical application of the methods proposed in this paper is shown in detail, aiming to provide guidelines for the practical design of this type of heat exchangers.

In this investigation, unless explicitly stated otherwise, 3D thermo-hydraulic numerical analyses with explicit simulation of heat exchanger pipes are conducted using COMSOL Multiphysics®.[7] The thermo-active piles studied here possess a length of $20m$ and are configured with a double U-loop pipe arrangement, as visually depicted in Fig. 1. The adopted domain spans dimensions of $80m$ by $80m$, consistently positioning the thermo-active pile(s) at the centre of it. The

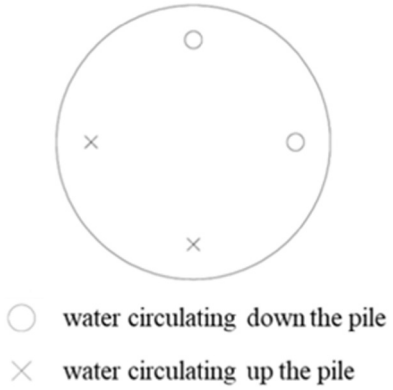

Fig. 1. Illustration of the double U-loop pipe arrangement adopted.

adopted depth of the domain is 40*m*. The domain size was checked through a sensitivity study and was found that these dimensions were sufficient to prevent any boundary effects. For the heat exchanger pipes, the concrete cover is 70*mm*, the inner diameter is 26.2*mm*, the pipe wall thickness is 2.9*mm*, and the fluid flow rate per U-loop is 1×10^{-4} $m^3 \bullet s^{-1}$ (which corresponds to a fluid velocity of $0.19m \bullet s^{-1}$). The thermo-active piles operate for 360 days and the ground temperature is assumed to be 20℃, a value which has been observed in dense urban areas (e.g. Bourne-Webb et al.[5]). However, it should be noted that, for the purpose of developing a design methodology, which is the objective of this paper, the initial ground temperature, assumed to be equal to that of the thermo-active piles, is not a determining factor. All domain boundaries are prescribed a thermal boundary condition where the temperature is not allowed to vary from its initial value. It is assumed the carrier fluid is water and Table 1 provides the thermal properties adopted for the pile concrete, soil and water. Additionally, when considering arrangements of piles within thermo-active pile groups, a regular rectangular array pattern is followed.

2. Simplified methodology for determining G-functions for thermo-active pile groups

This section commences with the evaluation of the G-function for a single thermo-active pile. Subsequently, the investigation extends to determining G-functions for two interacting thermo-active piles, spaced at varying distances. These analyses facilitate the assessment of how pile spacing impacts the increase in G-function values, and hence ground temperatures, resulting from thermal interference. This effect is subsequently quantified using a proposed empirical equation. The existence of this empirical equation enables the proposal of a simplified methodology for determining G-functions for thermo-active pile groups based on G-function for single piles. Finally, the validity of the empirical equation and the simplified methodology are confirmed through application to a 3×3 thermo-active pile group.

In this section, the G-functions are established by applying a constant heat flux of $100W \bullet m^{-1}$ to each pile. For a pile length of 20*m* and a double U-loop pipe arrangement, this corresponds to a heat flux of 2000*W* per pile or 1000*W* per U-loop. It is important to note that the G-functions are solely evaluated by calculating the average temperature along the surface of the pile shaft (i.e. at the pile edge), meaning that there is a loss of information on local variations in temperature – either circumferentially due to the position and number of heat exchange pipes (e.g. Loveridge & Powrie[23]) or along the pile due to heat losses through the ground surface or heat conduction towards the soil below the pile tip (e.g. Bourne-Webb et al.[5]). However, as a trade-off, this approach enables the determination of a single value which approximates the highest temperature to which the soil is subjected. In the COMSOL model, the pipe outlets are connected to the pipe inlets to form closed circuits, with the heat flux being introduced to the fluid before recirculation back into the ground, as illustrated in Fig. 2.

Table 1
Thermal properties adopted for pile concrete, soil and water.

	Pile	Soil	Water
Thermal conductivity $k\left[W \bullet m^{-1} \bullet K^{-1}\right]$	2.3	1.8	0.6
Volumetric heat capacity $\rho C_p \quad \left[kJ \bullet m^{-3} \bullet K^{-1}\right]$	1900	1800	4180

To demonstrate the independence of the method from the considered pile diameter, three distinct diameters – 600*mm*, 900*mm*, and 1800*mm* – are investigated. These values encompass the typical range of pile diameters commonly encountered in practical applications.[31] Note that it is assumed that the number of U-loops remain constant to enable a direct comparison in terms of the effect of the diameter. However, it would be expected that for the larger pile (diameter of 1800 *mm*) a larger number of pipes would be used.

2.1. Single pile

The analyses are conducted, and the average temperature rise at the pile edge is recorded and normalised into G-functions Φ_g, as per Eq. (2).[22] In this equation, k_{soil} $\left[W \bullet m^{-1} \bullet K^{-1}\right]$ represents the thermal conductivity of the soil, $\overline{P}$ $\left[W \bullet m^{-1}\right]$ is the applied heat flux per unit pile length, and ΔT_{wall} $[K]$ signifies the average change in pile wall temperature. The evolutions of the G-functions are plotted against time in Fig. 3 for all three pile diameters, both in terms of time (Fig. 3(a)) and Fourier number (Fig. 3(b)), the latter being defined in Eq. (3) where r_b is the radius of the pile.[22]

$$\Phi_g = \frac{2\pi k_{soil}}{\overline{P}} \Delta T_{wall} \tag{2}$$

$$Fo = \frac{k_{soil} \bullet t}{\rho_{soil} C_{p,soil} \bullet {r_b}^2} \tag{3}$$

Referring to Fig. 3, similar trends can be observed for all pile diameters. The pile heats up rapidly during the initial stages of heating due to the steep thermal gradient between the hot pipes and the cold pile. As time progresses and the pile continues to heat up, the thermal gradient is reduced, and the rate of heat transfer slows down. In effect, after one year of operation (Fig. 3(a)), the temperature increase reaches 90 % of that at steady state (Fig. 3(b)). It can also be observed that G-functions reduce with increasing pile diameters, indicating that increasing the pile diameter improves the thermal performance of the thermo-active pile (as explained in Section 1).

2.2. Two interacting piles

In this section, the G-functions for two interacting piles with varying spacing between them are investigated. The reduction in the power of two interacting piles (compared to that of a single pile) has been previously shown[21] to be better explained by the pile edge-to-pile edge (*ETE*) distance, rather than by the spacing factor (*SF*, defined as the pile centre-to-pile centre distance normalised by the pile diameter). However, as the value of *SF* is still widely used to describe pile groups, the geometries analysed in this paper are first formulated in terms of this quantity and then converted to *ETE*: as an example, for a 900*mm* diameter pile, *SF* values ranging from 2 to 12 in increments of 0.5 were considered, corresponding to *ETE* distances of $0.9m$ to $9.9m$ in increments of $0.45m$.

The analyses have been performed on all three pile diameters and the results are presented in Fig. 4. In Fig. 4, the results are depicted in terms of thermal interaction factor for G-functions TIF_G, a metric defined as the G-function for two interacting piles normalised by that of a single pile. It

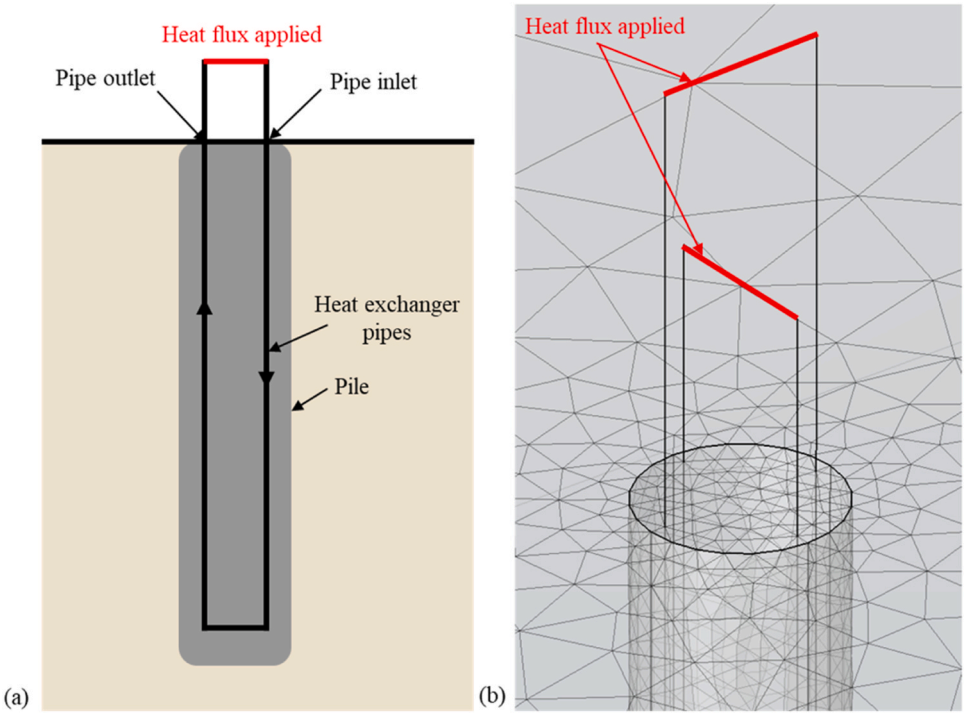

Fig. 2. Application of heat flux: (a) illustration of the approach and (b) implications to the numerical model.

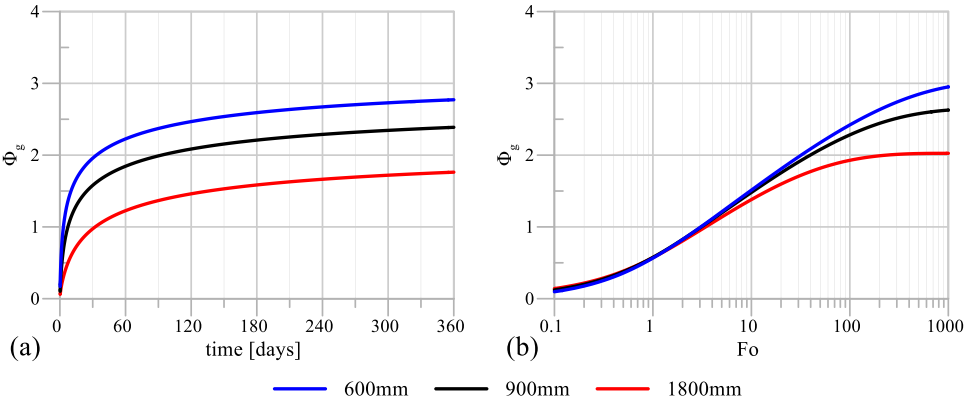

Fig. 3. G-functions for single piles with pile diameters of 600*mm*, 900*mm* and 1800*mm* as a function of (a) time and (b) Fourier number.

is important to note that, for brevity, only the results corresponding to *ETE* distances of 1.8*m*, 3.6*m*, 5.4*m*, 7.2*m* and 9*m* are presented.

Referring to Fig. 4, it can be observed that the TIF_G curves consistently remain above 1.0. This indicates that larger G-functions, or changes in pile edge temperature, are observed when two thermo-active piles interact with each other compared to the case of a single pile, as expected. Furthermore, for any considered pile diameter, higher TIF_G curves are obtained as the *ETE* distance is reduced. This aligns with expectations as the proximity of the two piles intensifies the effects of thermal interference, subjecting the pile edge to more significant temperature changes and, consequently, higher G-functions.

Fig. 4 also reveals that, for the same *ETE* distance, the TIF_G curve appears to be relatively independent of the pile diameter. Therefore, an empirical equation expressing TIF_G in terms of time $t[days]$ and $ETE[m]$ is proposed:

$$TIF_G(t,ETE) = \left[C_{G,1}\ln(ETE) + C_{G,2} + \frac{1-\left[C_{G,1}\ln(ETE)+C_{G,2}\right]}{1+\left(\frac{t}{A_G \bullet ETE}\right)^{B_{G,1}+B_{G,2}\bullet ETE}} \right]^{-1} \geq 1 \tag{4}$$

In Eq. (4), A_G, $B_{G,1}$, $B_{G,2}$, $C_{G,1}$ and $C_{G,2}$ are constants, which are calibrated using the least square methods, resulting in $A_G = 26.78$, $B_{G,1} = 0.4005$, $B_{G,2} = 0.4037$, $C_{G,1} = 0.1369$ and $C_{G,2} = 0.6640$. The shape chosen for Eq. (4) is that of the reciprocal of a modified hyperbolic formulation, such as the one used to describe the stiffness of a geomaterial by Taborda et al.[35]. When adopting this type of expression, the term $\left(C_{G,1}\ln(ETE)+C_{G,2}\right)^{-1}$ denotes the maximum value of the thermal interaction factor in the long-term (i.e. as $t \to \infty$). This means that it is possible to determine the maximum value of *ETE* beyond which no interaction between piles is considered by Eq. (4): $ETE_{\max} = \exp\left((1-C_{G,2})/C_{G,1}\right)$. For example, for the values given above, no thermal interaction is predicted for distances between piles above

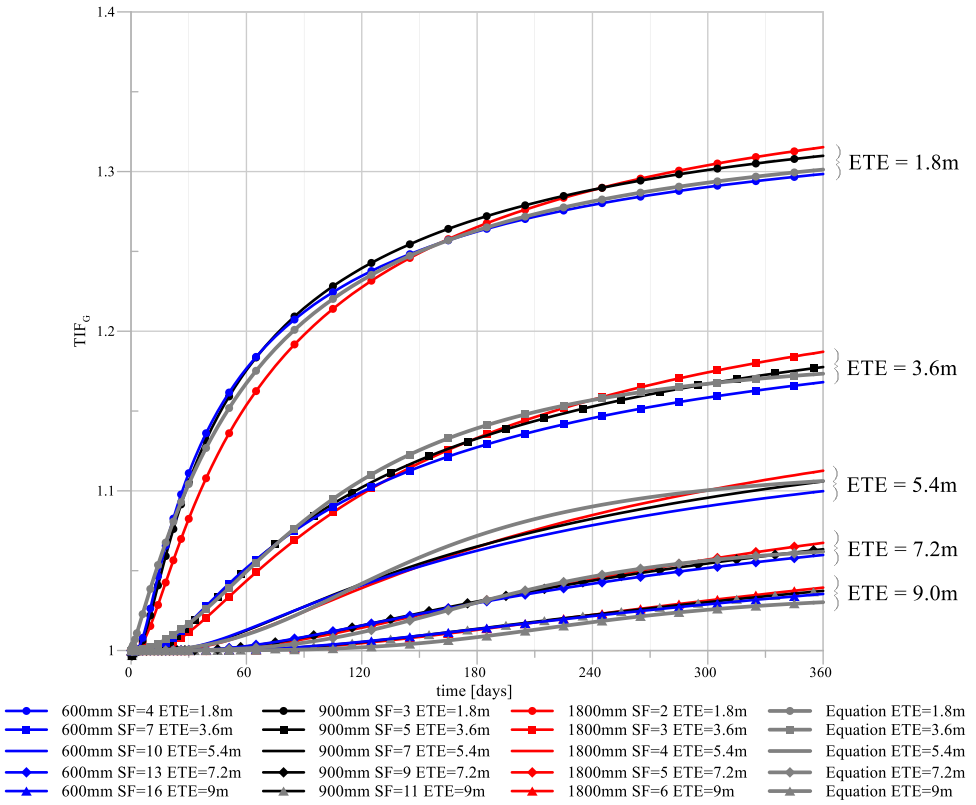

Fig. 4. Thermal interaction factor curves for two interacting thermo-active piles for pile diameters of 600*mm*, 900*mm* and 1800*mm*, and the corresponding curves fitted by Eq. (4).

$ETE_{\max} \approx 11.6m$. Furthermore, the term $A \bullet ETE$ determines the time at which the reciprocal of TIF_G rises to the midpoint between its initial value and its long term value, i.e. $t = A \bullet ETE \rightarrow TIF_G = \left(\left(1.0 + \left(C_{G,1}\ln(ETE) + C_{G,2}\right)\right)/2\right)^{-1}$. Clearly, the fact that this terms scales with ETE is hardly surprising, since a longer period of time is required for thermal interaction to take place between piles that are further away. Lastly, the term $B_{G,1} + B_{G,2} \bullet ETE$ denotes the non-linearity between time and the value of the thermal interaction factor, with smaller values of this term corresponding to smoother rises in this value. Based on the values above, the calibrated relationship suggests that the thermal interaction between two distant piles is limited, takes a longer period of time to start developing, but when it does happen, the thermal interaction factor builds up at a slightly faster rate. The TIF_G curves calculated using Eq. (4) are also plotted in Fig. 4 to illustrate the excellent fit with the numerical results. Clearly, the shown TIF_G curves are specific to a value of thermal conductivity of the soil. Therefore, in order to extend the applicability of the proposed methodology to cases where thermal conductivity of the soil may be different, the process outlined above was repeated for values of this property ranging between $0.9W \bullet m^{-1} \bullet K^{-1}$ (half the original value) and $3.6W \bullet m^{-1} \bullet K^{-1}$ (twice the original value). In Appendix A, the calibrated expressions for TIF_G are listed for each of the values of thermal conductivity, together with associated interpolation functions that allow the determination of TIF_G for any intermediate value of this property.

2.3. Simplified methodology

The availability of an empirical equation, as expressed in Eq. (4), which quantifies TIF_G curves solely in terms of time and ETE distances, enables the proposal of a simplified methodology for determining G-functions for thermo-active pile groups based on G-function of a single pile within the group, removing the need to perform specific analysis to evaluate the interaction between two piles. Since G-functions are linear quantities and can be superimposed[23,9], the G-function of a pile i within a pile group, denoted as $\Phi_{i,group}$, and comprising N_{piles} piles (subject to thermal interference from $(N_{piles} - 1)$ other piles), can be evaluated using Eq. (5):

$$\Phi_{i,group}(t) = \Phi_{single}(t) + \sum_{j=1}^{N_{piles}} \left[\Phi_{single}(t) \bullet TIF_G\left(t, ETE_j\right) - \Phi_{single}(t)\right]$$
$$= \Phi_{single}(t) \bullet \left[1 + \sum_{j=1}^{N_{piles}} \left[TIF_G\left(t, ETE_j\right) - 1\right]\right] \quad (5)$$

where it is assumed that $TIF_G(t, ETE_i) = 1.0$, i.e. the thermal interaction factor corresponding to pile i interacting with itself is 1.0. Moreover, in Eq. (5), the G-function of a pile within a pile group is determined by superimposing the effects from every other pile within the group. Note that this assumes that all the piles in the group have the same geometric characteristics, as is typically the case, and are described by the same G-function for a single pile, represented by Φ_{single}.

2.4. Validation

To validate the proposed empirical equation and the simplified methodology, the case of a 3 × 3 thermo-active pile group where piles are spaced apart by a spacing factor of 4 is considered. In this validation exercise, the G-functions for the piles at the corner, edge, and centre of the group, as well as the average G-function of the group are estimated. These estimations are based on the G-function of a single pile (determined numerically in Section 2.1), and are evaluated using the proposed empirical equation (Eq. (4)) and the simplified methodology outlined in Section 2.3. Subsequently, the estimated G-functions are compared with those determined numerically in COMSOL in Fig. 5(a), (b) and (c) for pile diameters of 600*mm*, 900*mm*, and 1800*mm*, respectively. It is important to note that, in these three configurations, values of edge-of-

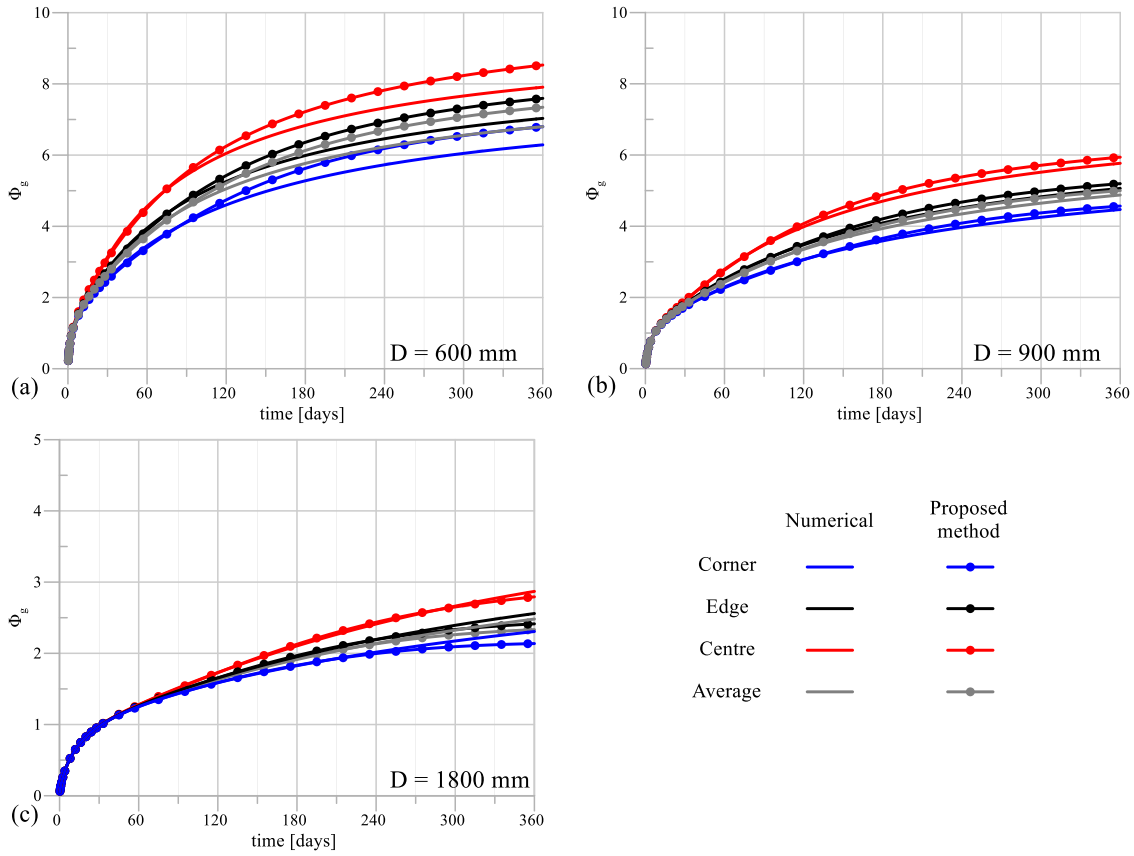

Fig. 5. Estimated and numerically determined G-functions for the 3 × 3 thermo-active pile group with pile diameters of (a) 600*mm*, (b) 900*mm*, and (c) 1800*mm*.

edge distance between 1.8 *m* (closest pile in a 3 ×3 group of 600 *mm* diameter piles with $SF = 4$) and 17.8 *m* (furthest pile in a 3 ×3 group of 1800 *mm* diameter piles with $SF = 4$) are considered, presenting a stern test for the proposed methodology.

The validation results presented in Fig. 5 reveal excellent agreement between the estimated G-functions and those determined numerically in COMSOL, with maximum errors of 8.3%, 4.0% and 7.3% for pile diameters of 600*mm*, 900*mm* and 1800*mm*, respectively. It is expected that the more significant errors observed in the group of smaller diameter piles is linked to the effect of the concrete cover, which, in proportion to the diameter, is larger in this case. Further validation exercises were performed for a wide range of pile arrangements, including 2 × 2, 4 × 4 and infinitely large pile groups. For brevity, these are shown in Appendix B. Overall, the good agreement obtained for all cases considered underscores the effectiveness and accuracy of both the empirical equation and the simplified methodology in estimating G-functions for thermo-active pile groups.

3. Power of thermo-active pile groups under transient thermal loads

A simplified methodology for estimating the power of thermo-active piles within thermo-active pile groups, based on the power of a single pile that constitutes the group, was developed by Liu & Taborda[21]. This method employs an empirically derived the thermal interaction factor for power, TIF_P, as described in Eq. (6), to quantify the power reduction on a thermo-active pile due to thermal interference from another nearby pile. Note that, similar to Eq. (4), this expression is based on a modified hyperbolic formulation such as the one adopted in Taborda et al.[35]. The observations regarding the roles of the terms in Eq. (4) that correspond to $\left(C_{P,1}\ln(ETE)+C_{P,2}\right)$, $(A_P \bullet ETE)$ and $\left(B_{P,1}+B_{P,2} \bullet ETE\right)$ remain valid for Eq. (6). In this equation, constants A_P, $B_{P,1}$, $B_{P,2}$, $C_{P,1}$ and $C_{P,2}$ have been determined as $A_P = 22.14$, $B_{P,1} = 0.4600$, $B_{P,2} = 0.3721$, $C_{P,1} = 0.1085$ and $C_{P,2} = 0.7317$. Similar to the thermal interaction factor for G-functions (Section 2.2), the curves for the thermal interaction factor for power are dependent on the thermal conductivity of the surrounding soil. Therefore, the analyses shown above were repeated for values of this property from $0.9W \bullet m^{-1} \bullet K^{-1}$ to $3.6W \bullet m^{-1} \bullet K^{-1}$. In Appendix A, the coefficients for the expression for TIF_P (Eq. (6)) were subsequently recalibrated for each of the values of thermal conductivity and interpolation functions are provided to allow the use of the proposed methodology for other values of this soil property. The power of thermo-active pile i within a thermo-active pile group, denoted as $\overline{P}_{i,group}$ $\left[W \bullet m^{-1}\right]$, can be evaluated using Eq. (7).

$$TIF_P(t,ETE) = C_{P,1}\ln(ETE) + C_{P,2} + \frac{1-\left[C_{P,1}\ln(ETE)+C_{P,2}\right]}{1+\left(\frac{t}{A_P \bullet ETE}\right)^{B_{P,1}+B_{P,2} \bullet ETE}} \leq 1.0 \qquad (6)$$

$$\overline{P}_{i,group}(t) = \overline{P}_{single}(t) \bullet \prod_{j=1}^{N_{piles}} TIF_P\left(t, ETE_j\right) \qquad (7)$$

Similar to Eq. (5), the thermal interaction factor corresponding to pile i interacting with itself is assumed to be $TIF_P(t, ETE_i) = 1.0$. Moreover, in Eq. (7), $\overline{P}_{single}$ $\left[W \bullet m^{-1}\right]$ represents the power of a single thermo-active pile unaffected by thermal interference, and N_{piles} is the number of piles within the group. However, this methodology is applicable only to cases with constant thermal loads. To extend the methodology for time-varying thermal loads, a temporal superposition technique[38] is adopted. In this case, Eq. (7) is modified into Eq. (8), where $\overline{P}_{i,group}$ has to be evaluated numerically. In Eq. (8), n represents the time step number being evaluated:

$$\overline{P}_{i,group}(t_n) = \sum_{k=1}^{n} \left\{ \left[\overline{P}_{single}(t_k) - \overline{P}_{single}(t_{k-1}) \right] \bullet \prod_{j=1}^{N_{piles}} TIF_P\left(t_n - t_{k-1}, ETE_j\right) \right\} \tag{8}$$

To validate the extended methodology, a 3 × 3 thermo-active pile group with 900*mm* pile diameter, which is subjected to transient thermal loads, is considered. In this validation exercise, the 3 × 3 thermo-active pile group is subjected to heating and cooling by a sinusoidal inlet temperature described by the function $T_{in}(t) = 20 + 20 \bullet \sin\left(\frac{2\pi t}{360}\right)$ [°C]. This simplified variation of inlet temperature has an amplitude of 20°C with a period of one year, oscillating around the initial ground temperature of 20°C, resulting in the fluid temperature varying between 0°C and 40°C. This is intended to represent an idealised operational pattern for a ground source energy system where the year is split equally between a cooling season (i.e. energy injected into the ground for 180 days) and a heating season (i.e. energy extracted from the ground for the remaining 180 days).

To apply the simplified method, the power of a single thermo-active pile, $\overline{P}_{single}$, subjected to the described thermal load has to be determined first. This determination is achieved through numerical analysis using COMSOL. Since the power of the thermo-active pile is determined based on the applied inlet temperature and the measured outlet temperature, the pipe arrangement adopted in this case is different from that illustrated in Fig. 2. This modified arrangement is illustrated in Fig. 6. Consequently, the power of the pile can be determined based on the applied inlet temperature, T_{in}, and the measured outlet temperature, T_{out}, as per Eq. (1). The numerical analysis is conducted, and the resulting evolution of $\overline{P}_{single}$ with time is presented in Fig. 7.

After obtaining $\overline{P}_{single}$, the extended simplified method is applied by evaluating Eqs. (6) and (8). Subsequently, the resulting time evolution of power for the piles at the corner, edge and centre of the group, as well as the average power of the group are compared with those obtained through numerical simulations in COMSOL. The comparisons are presented in Fig. 8(a)–(d), respectively.

The remarkable agreement observed between the power estimated using the simplified method and the numerical modelling in Fig. 8 clearly demonstrates the high degree of accuracy of the proposed approach when estimating the power of thermo-active pile groups while accounting for transient thermal loads. It is worth noting that the $\overline{P}_{single}$ used by the simplified method could have been determined through alternative means, such as field thermal response tests, empirical methods, or solely 2D numerical analyses using e.g. the simplified method developed by Liu & Taborda[20], rather than employing a full 3D analysis with heat exchanger pipes. The rationale for choosing full 3D analysis in this validation exercise is to eliminate any unnecessary approximations associated with the determination of $\overline{P}_{single}$. Moreover, detailed parametric studies – not shown here for brevity – indicate that, although computationally intensive due to the required number of steps, the accuracy of this method increases with the frequency of the variation of inlet temperature, rendering it a viable approach for analysing realistic operational patterns for heat pumps.

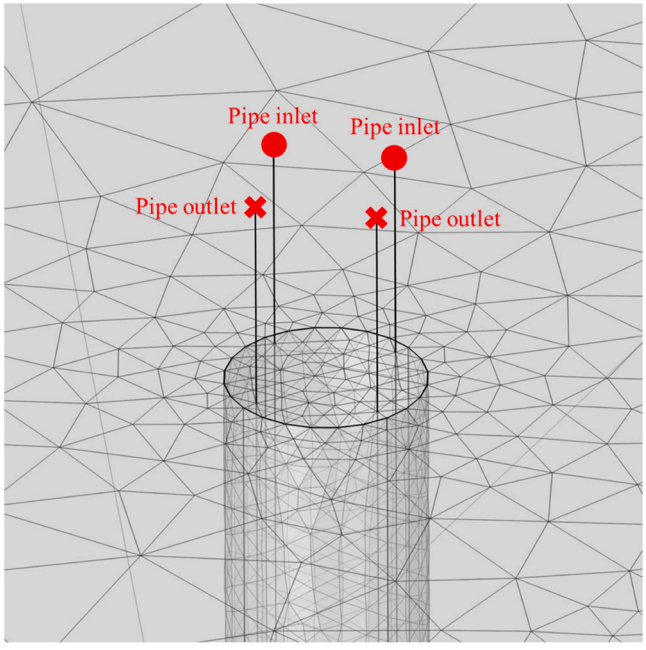

Fig. 6. Illustration of pipe arrangement when inlet temperatures are specified and power of pile is to be measured.

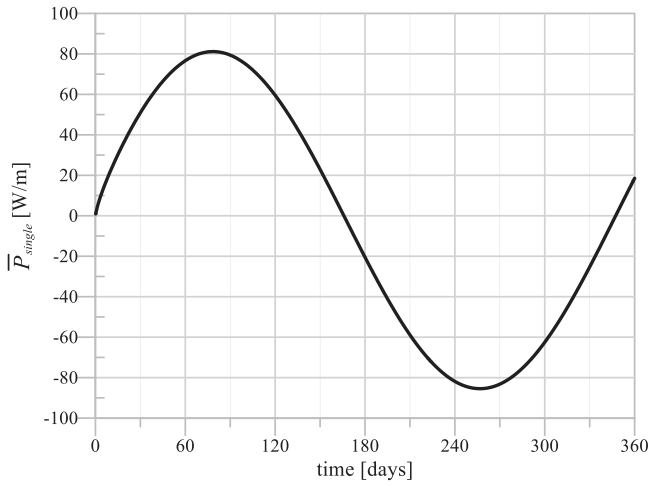

Fig. 7. Evolution of $\overline{P}_{single}$ with time for the single pile subjected to the time-varying thermal load obtained from the numerical model.

4. Practical application

Based on the methodologies proposed in the preceding sections, it is now possible to estimate both the power of piles within thermo-active pile groups ($\overline{P}_{i,group}$) and the temperature changes at the edges of the piles solely based on the applied inlet temperatures, which can be transient. This capability will be demonstrated in the following comprehensive validation exercise, which involves a 3 × 3 thermo-active pile group with piles spaced apart by a spacing factor of 4, installed in a soil which is initially at a temperature of $T = 20\,^{\circ}C$. These piles are subjected to a thermal load represented by an inlet temperature signal described by the function $T_{in}(t) = 20 + 20 \bullet \sin\left(\frac{2\pi t}{360}\right) + 10 \bullet \sin\left(\frac{2\pi t}{30}\right)$ [°C]. This inlet temperature signal is similar to the one considered in Section 3 but includes additional monthly cycles with an amplitude of 10°C. The validation exercise comprises the following calculation steps, which are visually depicted in the workflow chart presented in Fig. 9:

1. Calculate single pile power $\overline{P}_{single}$ from $T_{in}(t)$ (Section 4.1).
2. Convert to pile group power $\overline{P}_{i,group}$ from $\overline{P}_{single}$ (Section 4.2).
3. Establish single pile G-function Φ_{single} (Section 4.3).
4. Assemble pile group G-function $\Phi_{i,group}$ from Φ_{single} (Section 4.4).
5. Determine changes in pile wall temperature by combining $\overline{P}_{i,group}$ from Step 2 with $\Phi_{i,group}$ from Step 4 (Section 4.5).

Throughout all these steps, the results obtained from the simplified

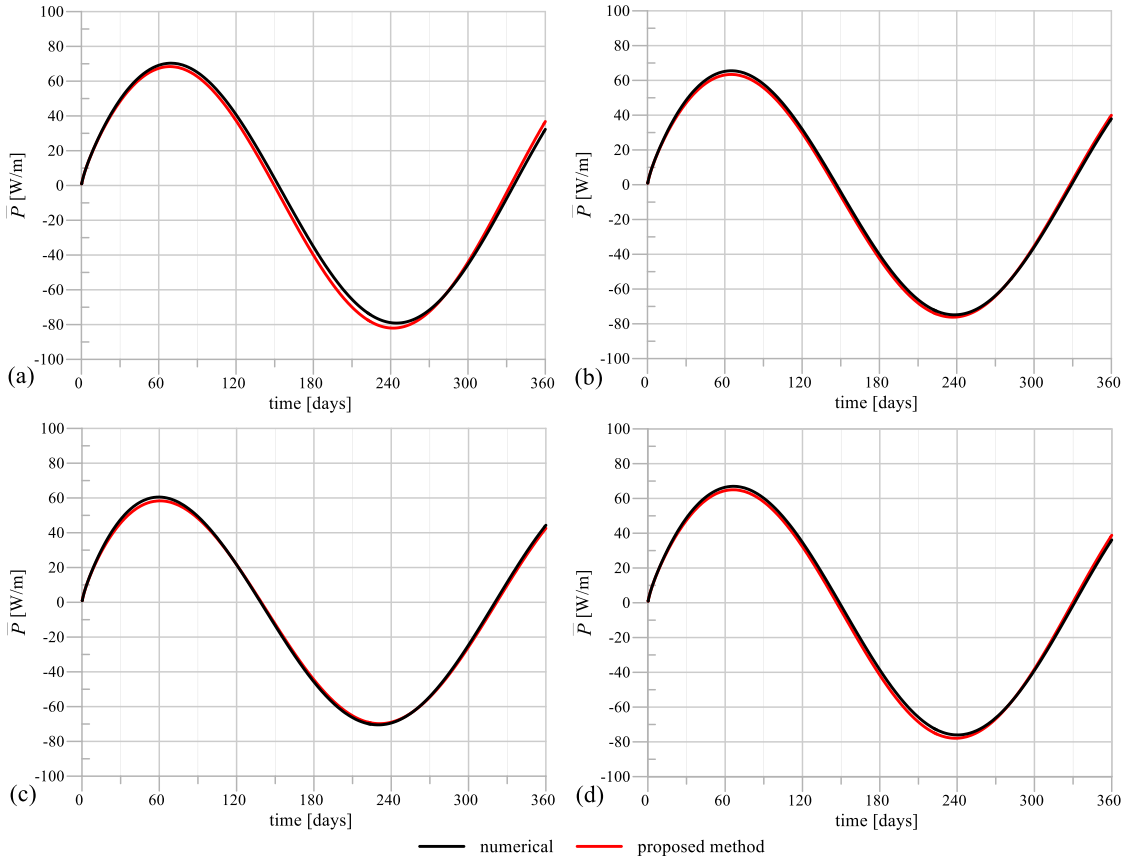

Fig. 8. Time evolution of power for the (a) corner, (b) edge, and (c) centre piles, as well as the (d) average power within the 3 × 3 thermo-active pile group, estimated using the proposed method and compared with numerical simulation results obtained in COMSOL.

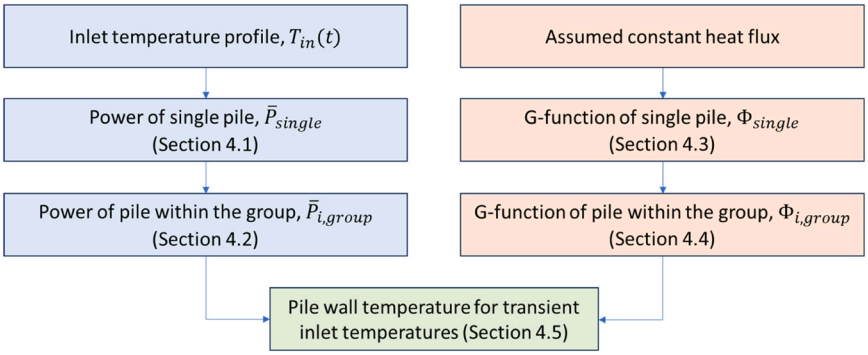

Fig. 9. Workflow chart for the validation exercise.

method are consistently compared against those generated from numerical modelling using full 3D COMSOL analyses.

4.1. Determination of $\overline{P}_{single}$ from $T_{in}(t)$

To determine the power of a single thermo-active pile ($\overline{P}_{single}$) based on the applied inlet temperature ($T_{in}(t)$), the simplified methodology from Liu & Taborda[21], which avoids carrying out 3D transient thermo-hydraulic analysis with explicit modelling of heat exchanger pipes, is employed. This method requires only a 2D thermal analysis of the pile cross-section and the surrounding soil, while the thermal load is imposed as a temperature boundary condition at the locations of the heat exchanger pipes. The evolution of the average temperature along the circumference with radius $r = r_{pipes}$ (where r_{pipes} is the radial distance between the centre of thermo-active pile and the centre of heat exchanger pipes) is determined. This evolution of the average temperature is then used as a temperature boundary condition within the pile at $r = r_{pipes}$ in an axisymmetric thermal analysis. The power of the pile is subsequently calculated by assessing the change in energy content of the system, along with the energy lost through the system's boundaries. Liu & Taborda[21] presented an in-depth description of this methodology, as well as an assessment of its performance.

For reference, the $\overline{P}_{single}$ determined using the simplified method is compared in Fig. 10 with the results obtained using 3D thermo-hydraulic analysis as described in Section 3. It is evident from Fig. 10 that there is a good agreement between the two approaches with the simplified method requiring less sophisticated and computationally intensive analyses. The maximum error observed in terms of peak power

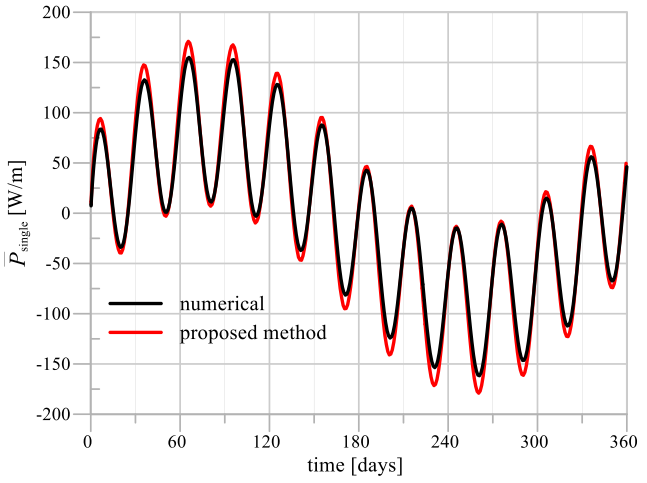

Fig. 10. Comparison of $\overline{P}_{single}$ estimated using the proposed method with 3D thermo-hydraulic analysis.

is limited to about 10%.

4.2. Determination of $\overline{P}_{i,group}$ from $\overline{P}_{single}$

Following the determination of $\overline{P}_{single}$, the power of piles within the 3 × 3 thermo-active pile group ($\overline{P}_{i,group}$) can be estimated using Eqs. (6) and (8). The resulting time evolution of power for the piles at the corner, edge and centre of the group, as well as the average power of the group are compared with those obtained through numerical simulations in COMSOL. The comparisons are illustrated in Fig. 11 (a)–(d), respectively.

Referring to Fig. 11, it is evident that there is a generally good agreement between the estimations from the simplified method and the results obtained from numerical analyses, with a maximum error in terms of peak power of up to 20 %. It is worth noting that the larger error observed during the estimation of $\overline{P}_{i,group}$, compared to that of $\overline{P}_{single}$, can be attributed to the accumulation of errors in the process, as $\overline{P}_{single}$ used to obtain $\overline{P}_{i,group}$ was itself obtained using an approximate methodology.

4.3. Determination of G-function for a single pile Φ_{single}

To compute efficiently the G-function for a single thermo-active pile, an axisymmetric analysis is performed. In this analysis, a heat flux of $2000W$ (equivalent to $100W \bullet m^{-1}$) is applied over a shell within the pile located at a radial distance equal to that of the heat exchanger pipes (i.e. at $r = r_{pipes}$), while the average temperature at the pile edge is monitored over time. Subsequently, the evolution of the average temperature over time is normalised into a G-function (Φ_{single}) according to Eq. (2) and is compared in Fig. 12 to the results obtained through a 3D thermo-hydraulic analysis in COMSOL, of the type described in Section 2. Clearly, while there is a considerable difference in the complexity of the two analyses, the obtained results are very similar, with a maximum error of up to 5 %.

4.4. Determination of G-function of a pile within the group $\Phi_{i,group}$ from Φ_{single}

After establishing Φ_{single}, the G-functions of piles within the 3 × 3 thermo-active pile group ($\Phi_{i,group}$) can be estimated using Eqs. (4) and (5). The resulting G-functions for the piles at the corner, edge and centre

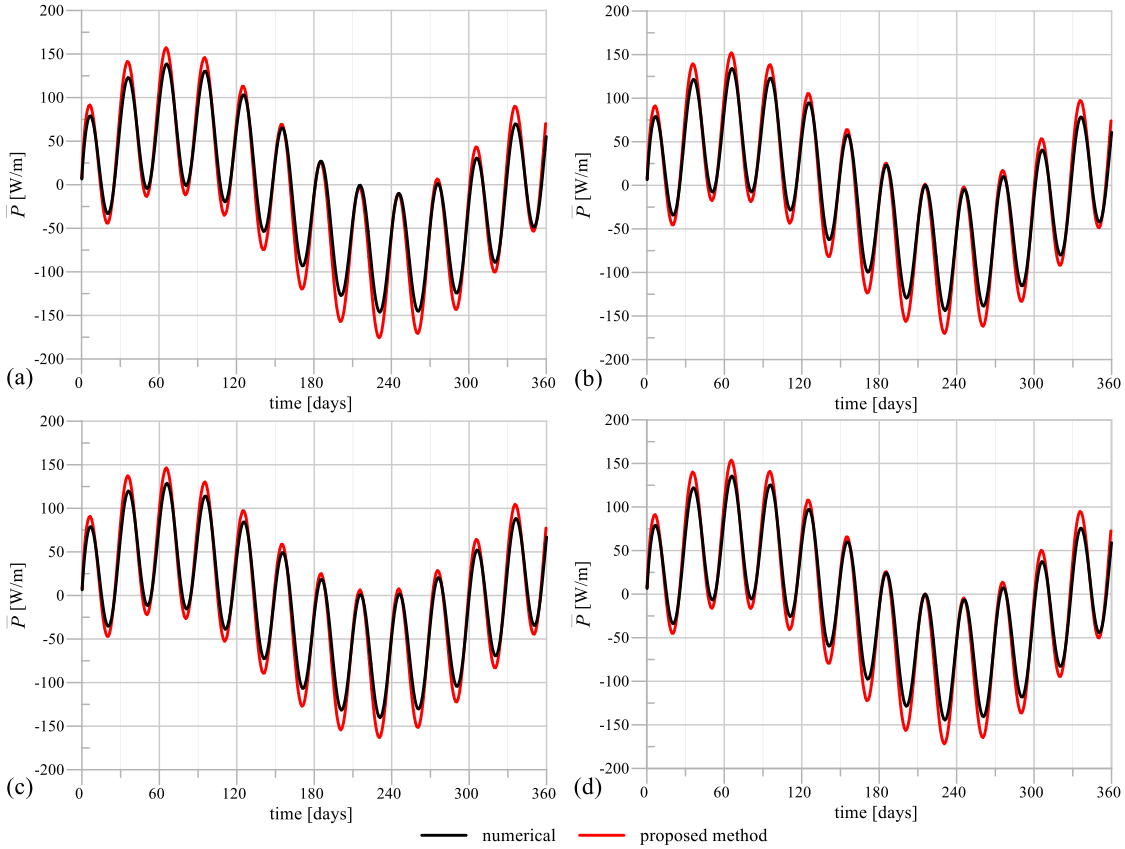

Fig. 11. Comparison of $\overline{P}_{i,group}$ estimated using the proposed method with results obtained from numerical simulation in COMSOL for the (a) corner, (b) edge, and (c) centre piles of the 3 × 3 group, as well as the (d) average power of the group.

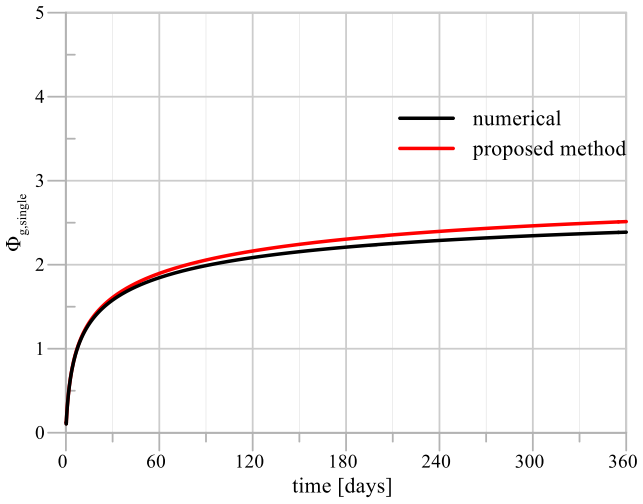

Fig. 12. Comparison of Φ_{single} estimated using the proposed method with numerical simulation results obtained in COMSOL.

of the group, as well as the average G-function of the group are compared with those determined through 3D thermo-hydraulic analyses in COMSOL. These comparative results are presented in Fig. 13 (a)–(d), respectively.

Referring to Fig. 13, it is evident that there is a notable agreement between the two approaches to obtain G-functions, with the error being limited to about 9 %. It is worth noting that this error is slightly larger than that associated with Φ_{single} estimation, as the error from Φ_{single} estimation has been propagated during the estimation of $\Phi_{i,group}$.

4.5. Determination of changes in pile wall temperature from $\overline{P}_{i,group}$ and $\Phi_{i,group}$

With knowledge of the power ($\overline{P}_{i,group}$) and G-function ($\Phi_{i,group}$) of the piles within the 3 × 3 thermo-active pile group, it is possible to determine the average changes in temperature at the pile edge (ΔT_{wall}). However, as power varies with time, the temporal superposition technique used in e.g. Loveridge & Powrie[22] has to be applied to calculate numerically the change in temperature at the pile edge using Eq. (9). In Eq. (9), n represents the time step number being evaluated.

$$\Delta T_{wall}(t_n) = \sum_{k=1}^{n} \frac{\overline{P}(t_k)}{2\pi k_{soil}} \left[\Phi_g(t_n - t_{k-1}) - \Phi_g(t_n - t_k) \right] \tag{9}$$

The ΔT_{wall} for the pile at the corner, edge and centre of the 3 × 3 group, as well as the average ΔT_{wall} of the entire group, are determined and compared against those obtained using 3D thermo-hydraulic analysis in Fig. 14 (a)–(d), respectively.

Referring to Fig. 14, it is clear that the estimated evolutions of ΔT_{wall} align reasonably well with those obtained from COMSOL simulations. The time-averaged absolute error remains limited to 1.6℃, demonstrating that throughout the entire period of analysis, temperature deviations are generally very small. Nevertheless, it is essential to note that for specific time instants, primarily associated with the estimation of extreme values of temperature, errors could potentially extend up to 25 %. This larger error is perhaps unsurprising as $\overline{P}_{single}$, $\overline{P}_{i,group}$, Φ_{single}, and $\Phi_{i,group}$ were all estimated using simplified methods, resulting in the accumulation of minor discrepancies. In effect, if $\overline{P}_{single}$ and Φ_{single} were

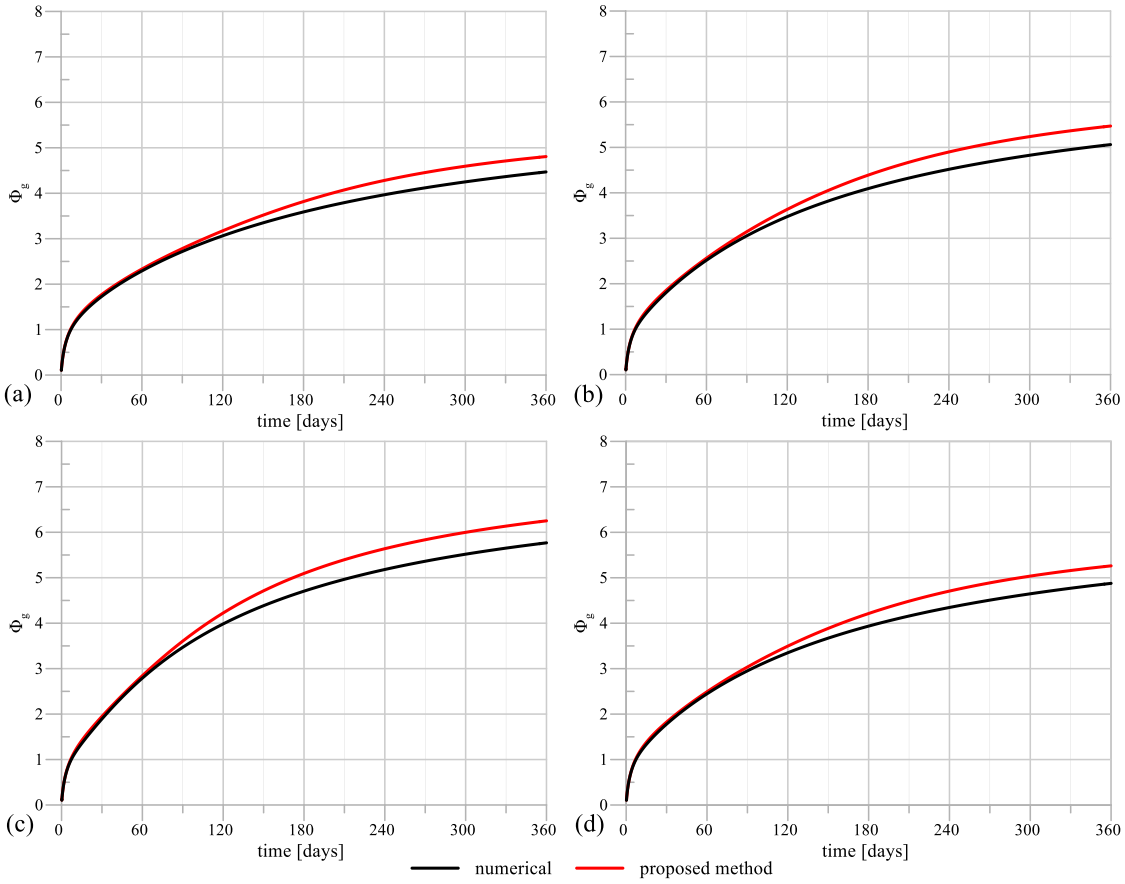

Fig. 13. Comparison of $\Phi_{i,group}$ estimated using the proposed method with results obtained from numerical simulation in COMSOL for the (a) corner, (b) edge, and (c) centre piles of the 3 × 3 group, as well as the (d) average G-function of the group.

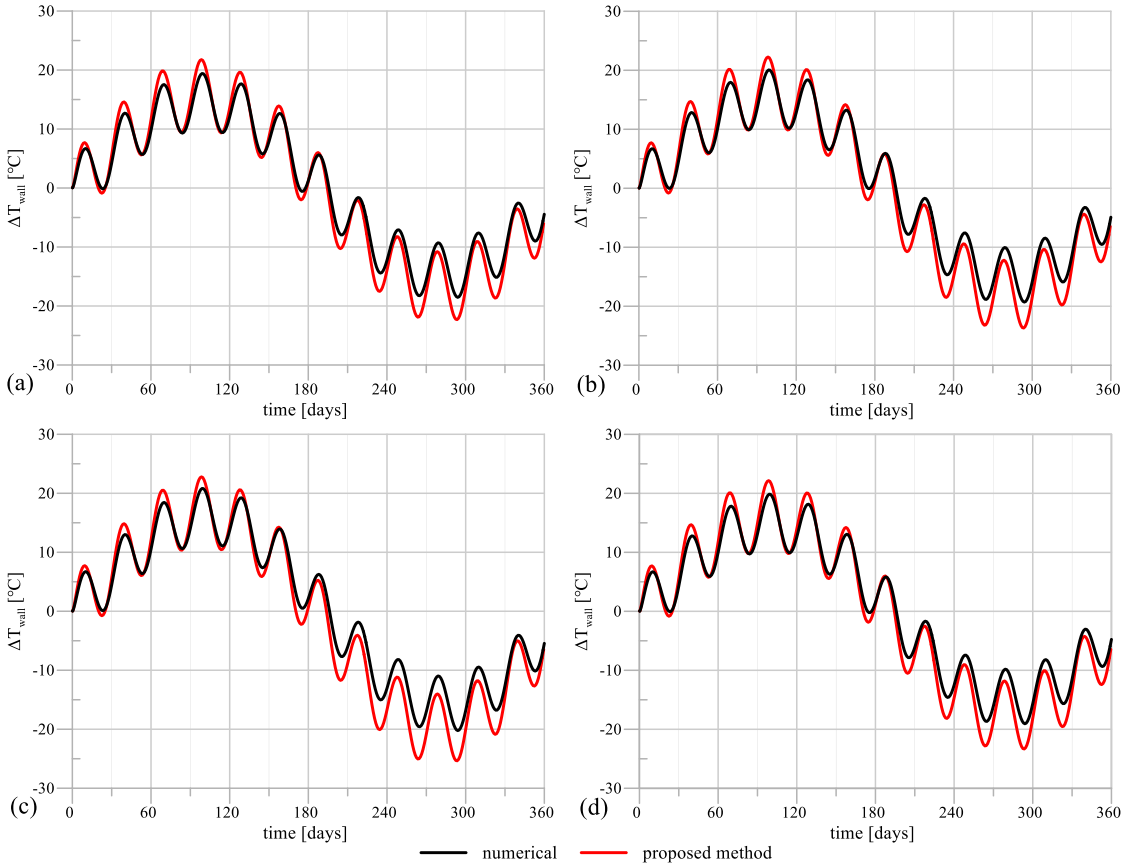

Fig. 14. Comparison of ΔT_{wall} estimated using $\overline{P}_{i,group}$ and $\Phi_{i,group}$ from proposed methods with results obtained from numerical simulation in COMSOL for the (a) corner, (b) edge, and (c) centre piles of the 3 × 3 group, as well as the (d) average ΔT_{wall} of the group.

derived numerically, the observed error in estimating extreme temperature values would drop to values below 10 %.

This comprehensive validation exercise has demonstrated the effectiveness of simplified methodologies for assessing the thermal performance of both individual thermo-active piles and thermo-active pile groups. With these established methods, the power and changes in temperature at the pile edge for piles within thermo-active pile groups can be accurately determined, relying solely on the input of the inlet temperature signal. Notably, this process does not necessitate computationally expensive 3D analyses or the simulation of heat exchanger pipes. These advancements open up new avenues for efficient and reliable thermal performance assessments in thermo-active pile systems.

5. Conclusions

In this paper, a comprehensive and novel suite of simplified methodologies is introduced, meticulously designed to evaluate the thermal performance of thermo-active pile groups. Firstly, a simplified method is introduced for the determination of G-functions concerning piles within thermo-active pile groups, building upon the G-function of a single thermo-active pile which is unaffected by thermal interference. Employing an empirically derived thermal interaction factor for G-functions, this technique quantifies the increase in G-function when a pile is subjected to thermal interference from another nearby pile. The principle of superposition then allows for the thermal interference from multiple piles to be quantified in a thermo-active pile group.

Furthermore, an approach for determining the power of piles within thermo-active pile groups is extended to accommodate time-varying thermal loads. This method establishes an empirically derived thermal interaction factor for power to account for reductions in power incurred when a pile is subjected to thermal interference from another pile operating in its vicinity. Through the application of a temporal superposition technique, the power of the pile when subjected to thermal interference from multiple piles in a thermo-active pile group can be determined.

The strength of these methodologies lies in their efficiency and versatility, as they do not necessitate computationally expensive 3D analyses or simulation of heat exchanger pipes, and can be applied to pile groups with any pile configuration. To validate their efficacy, a rigorous validation exercise is undertaken, involving a 3 × 3 thermo-active pile group subjected to a time-varying thermal load. Remarkably, relying solely on the time-varying inlet temperature signal, excellent estimations of power, G-function, and changes in temperature at the edges of the piles within the pile group are achieved.

Clearly, these simplified methodologies offer a robust framework for evaluating the thermal performance of thermo-active pile groups, providing valuable insights for the design and optimisation of thermo-active pile systems.

CRediT authorship contribution statement

David M.G. Taborda: Conceptualization, Funding acquisition, Methodology, Supervision, Writing – review & editing. **Ryan Yin Wai Liu:** Conceptualization, Investigation, Methodology, Validation, Writing – original draft.

Declaration of Competing Interest

The authors declare the following financial interests/personal relationships which may be considered as potential competing interests:

Ryan Yin Wai Liu reports financial support was provided by Engineering and Physical Sciences Research Council. David Taborda reports financial support was provided by Engineering and Physical Sciences Research Council. If there are other authors, they declare that they have no known competing financial interests or personal relationships that could have appeared to influence the work reported in this paper.

Data availability

Data will be made available on request.

Acknowledgements

This research is part of the SaFEGround (Sustainable, Flexible and Efficient Ground-source heating and cooling systems) project, which is funded by the Engineering and Physical Sciences Research Council (EPSRC) (grant number: EP/V042149/1).

Appendix A. Dependency of thermal interaction factors on soil thermal conductivity

To evaluate the impact of the thermal conductivity of the soil on the thermal interaction factors for G-functions (TIF_G) and power (TIF_P), multiple COMSOL analyses were performed using values of this property ranging from $0.9W \bullet m^{-1} \bullet K^{-1}$ (i.e. half the value used in the original analyses in this paper) to $3.6W \bullet m^{-1} \bullet K^{-1}$ (i.e. twice the value used in the original analyses). The analytical expressions for these thermal interaction factors, expressed by Eqs. (4) and (6), were subsequently calibrated, leading to the constants reported in Tables A.1 and A.2 for TIF_G and TIF_P, respectively. For intermediate values of thermal conductivity, interpolation functions listed in Tables A.3 can be used, extending the applicability of the method described in this paper to a wider range of scenarios involving soil thermal conductivities different from the value considered in this study ($1.8W \bullet m^{-1} \bullet K^{-1}$). Note that the thermal interaction factors were computed for thermo-active piles with two U-loops, while it would be expected that, at least for the 1800 *mm* pile, a larger number of U-loops would be used. Although a parametric study reported in Liu & Taborda (2014) suggests that the density of heat sources has only a minor effect on the thermal interaction factors, it is possible that a recalibration of the expressions proposed in this paper would be required to prevent additional, unnecessary inaccuracies.

Table A1
Coefficients for the expression for TIF_G (Eq. (4)).

k_{soil}(W m^{-1} K^{-1})	A_G	$B_{G,1}$	$B_{G,2}$	$C_{G,1}$	$C_{G,2}$
0.9	42.31	0.4542	0.5551	0.1324	0.7039
1.8 (original case)	26.78	0.4005	0.4037	0.1369	0.6640
2.7	19.11	0.1721	0.4888	0.1470	0.6433
3.6	15.17	0.1509	0.4545	0.1485	0.6316

Table A2
Coefficients for the expression for TIF_P (Eq. (6)).

k_{soil}(W m^{-1} K^{-1})	A_P	$B_{P,1}$	$B_{P,2}$	$C_{P,1}$	$C_{P,2}$
0.9	29.86	0.1897	0.6508	0.1290	0.7195
1.8 (original case)	22.14	0.4600	0.3721	0.1085	0.7317
2.7	16.66	0.3755	0.4238	0.09854	0.7523
3.6	14.28	0.4377	0.3746	0.08914	0.7690

Table A3
Interpolation functions for the coefficients of TIF_G (Eq. (4)) and TIF_P (Eq. (6)).

Coefficient	TIF_G (Eq. (4))	TIF_P (Eq. (6))
A_G, A_P	$39.43\ k_{soil}^{-0.737}$	$28.26\ k_{soil}^{-0.532}$
$B_{G,1}$, $B_{P,1}$	$0.3997\ k_{soil}^{-0.811}$	$0.2045\ k_{soil}^{0.606}$
$B_{G,2}$, $B_{P,2}$	$-0.03860\ k_{soil} + 0.5953$	$0.6259\ k_{soil}^{-0.397}$
$C_{G,1}$, $C_{P,1}$	$0.01190\ln k_{soil} + 0.1345$	$-0.02900\ln k_{soil} + 0.1266$
$C_{G,2}$, $C_{P,2}$	$0.6969\ k_{soil}^{-0.079}$	$0.01850\ k_{soil} + 0.7020$

Appendix B. Validation of the proposed method for other geometric configuration

To evaluate the performance of the proposed method for a wide range of geometries, three additional cases corresponding to a spacing factor (SF) of 4 were investigated: a small 2×2 pile group, a large 4×4 pile group and, as an extreme case, an infinitely large pile group. For simplicity, in these three scenarios all the piles had the same characteristics as those in the 3×3 pile group discussed in Section 2.4 subjected to the same type of thermal load (constant heating for one year). The results are shown in Figure B.1, where a very good agreement can be seen between the proposed method and the corresponding thermo-hydraulic analyses performed in COMSOL. Note that, for the infinitely large pile group, a group of 7×7 was used, since any additional piles beyond these would be predicted to have no influence on the central pile of the group. In COMSOL, an infinitely large pile group is modelled according to the methodology shown in Liu & Taborda.[21].

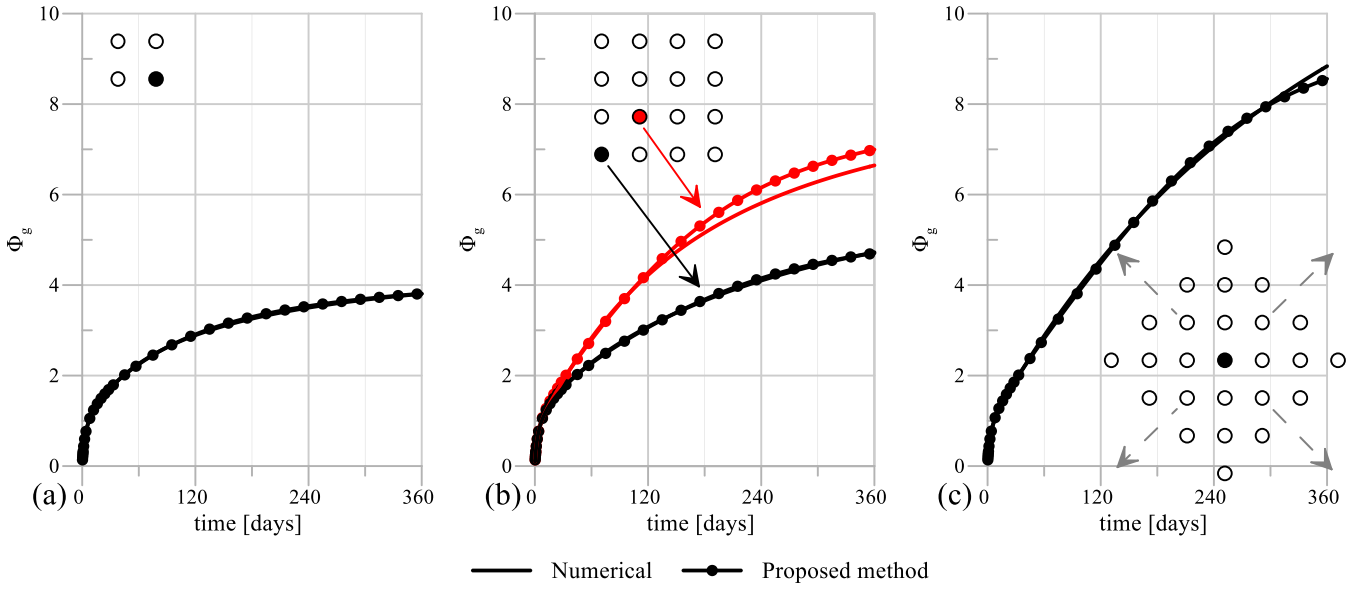

Figure B.1. Estimated and numerically determined G-functions for 900*mm* diameter thermo-active piles arranged with $SF = 4$ in (a) 2×2, (b) 4×4 and (c) infinitely large groups.

.

References

1. Alberdi-Pagola M, Poulsen SE, Jensen RL, Madsen S. Thermal design method for multiple precast energy piles. *Geothermics*. 2019;78:201–210.
2. Amatya BL, Soga K, Bourne-Webb PJ, Amis T, Laloui L. Thermo-mechanical behaviour of energy piles. *Geotechnique*. 2012;62(6):503–519.
3. Amis A, Loveridge F. Energy piles and other thermal foundations for gshp–developments in Uk practice and research. *Rehva J*. 2014;2014(1):32–35.
4. Brandl H. Energy foundations and other thermo-active ground structures. *Geotechnique*. 2006;56(2):81–122.
5. Bourne-Webb PJ, Amatya B, Soga K, Amis T, Davidson C, Payne P. Energy pile test at lambeth college, london: geotechnical and thermodynamic aspects of pile response to heat cycles. *Géotechnique*. 2009;59(3):237–248.
6. Bourne-Webb PJ, Amatya B, Soga K. A framework for understanding energy pile behaviour. *Proc Inst Civ Eng - Geotech Eng*. 2013;166(2):170–177.
7. COMSOL A.B., *COMSOL Multiphysics Version 6.0*, ⟨www.comsol.com⟩. COMSOL AB, Stockholm, Sweden; 2022.
8. Di Donna A, Laloui L. Numerical analysis of the geotechnical behaviour of energy piles. *Int J Numer Anal Methods Geomech*. 2015;39(8):861–888.
9. Eskilson P. *Thermal Analysis of Heat Extraction Boreholes* (PhD thesis). Sweden: University of Lund,; 1987.
10. Gao J, Zhang X, Liu J, Li K, Yang J. Numerical and Experimental Assessment of Thermal Performance of Vertical Energy Piles: An Application. *Appl Energy*. 2008;85(10):901–910.
11. Gawecka KA, Taborda DMG, Potts DM, Cui WJ, Zdravkovic L, Kasri MSH. Numerical modelling of thermo-active piles in London Clay. *Proc Inst Civ Eng-Geotech Eng*. 2017;170(3):201–219.
12. Go GH, Yoon S, Park DW, Lee S-R. Thermal behavior of energy pile considering ground thermal conductivity and thermal interference between piles. *J Korean Soc Civ Eng*. 2013;33(6).
13. Iodice C, Di Laora R, Tamagnini C, Viggiani GMB, Mandolini A. Numerical analysis of energy piles in a hypoplastic soft clay under cyclic thermal loading. *Int J Numer Anal Methods Geomech*. 2023;47(7):1175–1201.
14. Jensen-Page L, Loveridge F, Narsilio GA. Thermal response testing of large diameter energy piles. *Energies*. 2019;12(14).
15. Kong G, Sun Z, Wang Y, Yang Q. Group performance of multiple series-connected energy piles under thermal loading. *Case Stud Therm Eng*. 2023:43.
16. Kong L-P, Qiao L, Xiao Y-Y, Li Q-W. A study on heat transfer characteristics and pile group influence of enhanced heat transfer energy piles. *J Build Eng*. 2019:24.
17. Laloui L, Nuth M, Vulliet L. Experimental and numerical investigations of the behaviour of a heat exchanger pile. *Int J Numer Anal Methods Geomech*. 2006;30(8):763–781.
18. Liu RYW, Sailer E, Taborda DMG & Potts DM. Evaluating the impact of different pipe arrangements on the thermal performance of thermo-active piles. In: *Proceedings of the 2nd International Conference on Energy Geotechnics ICEGT 2020*. San Diego, USA; 2020.
19. Liu RYW, Taborda DMG. In: Zdravkovic L, Kontoe S, Taborda DMG, Tsiampousi A, eds. *Thermal performance of thermo-active pile groups*. London, United Kingdom: NUMGE 2023; 2023.
20. Liu RYW, Taborda DMG. A simplified methodology for determining the thermal performance of thermo-active piles. *Environ Geotech (Print)*. 2023. https://doi.org/10.1680/jenge.22.00119.
21. Liu RYW, Taborda DMG. The effects of thermal interference on the thermal performance of thermo-active pile groups. *Renew Energy*. 2024;225, 120357. https://doi.org/10.1016/j.renene.2024.120357.
22. Loveridge F, Powrie W. Temperature response functions (G-Functions) for single pile heat exchangers. *Energy*. 2013;57:554–564.
23. Loveridge F, Powrie W. G-functions for multiple interacting pile heat exchangers. *Energy*. 2014;64:747–757.
24. Loveridge F, Schellart A, Rees S, et al. Heat recovery and thermal energy storage potential using buried infrastructure in the Uk. *Proc Inst Civ Eng - Smart Infrastruct Constr*. 2022;175(1):10–26.
25. Lyu W, Pu H, Chen J. Thermal performance of an energy pile group with a deeply penetrating U-shaped heat exchanger. *Energies*. 2020;13(21).
26. Merton Council (2010) Sustainable design and construction evidence base: climate change in the planning system. Merton Council.
27. Ng CWW, Farivar A, Gomaa SMMH, Shakeel M, Jafarzadeh F. Performance of elevated energy pile groups with different pile spacing in clay subjected to cyclic non-symmetrical thermal loading. *Renew Energy*. 2021;172:998–1012.
28. Ng CWW, Shi C, Gunawan A, Laloui L. Centrifuge modelling of energy piles subjected to heating and cooling cycles in clay. *Geotech Lett*. 2014;4(4):310–316.
29. Ng CWW, Shi C, Gunawan A, Laloui L, Liu HL. Centrifuge modelling of heating effects on energy pile performance in saturated sand. *Can Geotech J*. 2015;52(8):1045–1057.
30. Park S, Lee D, Lee S, Chauchois A, Choi H. Experimental and numerical analysis on thermal performance of large-diameter cast-in-place energy pile constructed in soft ground. *Energy*. 2017;118:297–311.
31. Rutty PC. Piling in London – a HistoryHiggins KG, Ainsworth Y, Toll DG, Osman AS, eds. *Piling 2020*. 2021:451–457.
32. Sailer E, Taborda DMG, Zdravkovic L. A new approach to estimating temperature fields around a group of vertical ground heat exchangers in two-dimensional analyses. *Renew Energy*. 2018;118:579–590.
33. Sani AK, Singh RM, Amis T, Cavarretta I. A review on the performance of geothermal energy pile foundation, its design process and applications. *Renew Sustain Energy Rev*. 2019;106:54–78.
34. Stewart MA, McCartney JS. Centrifuge modeling of soil-structure interaction in energy foundations. *J Geotech Geoenviron Eng*. 2014;140(4):04013044.
35. Taborda DMG, Potts DM, Zdravkovic L. On the assessment of energy dissipated through hysteresis in finite element analysis. *Comput Geotech*. 2016;71:180–194.
36. Tiwari AK, Kumar A, Basu P. The influence of thermal interaction on energy harvesting efficiency of geothermal piles in a group. *Appl Therm Eng*. 2022:200.
37. World Wide Fund For Nature. Climate Mitigation by Merton Rule, 2019. Available from: ⟨https://wwf.panda.org/?204444/Merton-London-climate-rule⟩ [Accessed: 20th February 2020].

38. Yavuzturk C, Spitler JD. A short time step response factor model for vertical ground loop heat exchangers. *ASHRAE Trans*. 1999;105(2):475–485.
39. You S, Cheng X, Guo H, Yao Z. In-situ experimental study of heat exchange capacity of C.F.G. Pile geothermal exchangers. *Energy Build*. 2014;79:23–31.
40. Zhao Q, Chen B, Tian M, Liu F. Investigation on the thermal behavior of energy piles and borehole heat exchangers: a case study. *Energy*. 2018;162:787–797.